European Rotorcraft Forum

Numerical investigation of wing-propeller aerodynamic interaction through a vortex particle-based aerodynamic solver

Alberto Savino*, Alessandro Cocco, Alex Zanotti,
Politecnico di Milano, Dipartimento di Scienze e Tecnologie Aerospaziali,
via La Masa 34, 20156, Milano - Italy
* alberto.savino@polimi.it

Vincenzo Muscarello
RMIT University, School of Engineering, Aerospace Engineering and Aviation,
264 Plenty Rd, 3082, Melbourne - Australia

Abstract

The present paper describes the results of a numerical investigation of a wing with an integrated propeller using the mid-fidelity aerodynamic solver DUST. The wing/propeller model considered in this work was widely investigated in literature both by experiments and high-fidelity CFD simulations and represents a classical benchmark case for the aerodynamic study of tiltrotors and electrical distributed propulsion aircraft configurations. The present numerical activity showed the capabilities of a mid-fidelity aerodynamic solver based on the vortex particle method, such as DUST, to capture the aerodynamic interactional effects of the installed propeller on the wing by a direct comparison of wing pressure coefficient distributions and propeller airloads with both experimental data and high-fidelity CFD simulations. Moreover, the instantaneous representation of the flow field between the propeller and the wing, as well as the pressure fluctuations on the wing surface, highlighted the capabilities to build a robust aerodynamic model of the wing/propeller in DUST aimed at studying the aeroacoustic aspects of such a complex configuration typical of Advanced Air Mobility aircraft configurations.

1 Introduction

The numerical investigation of the complex aerodynamics characterizing tiltrotors or distributed electrical propulsion aircraft is a great challenge for Computational Fluid Dynamics (CFD) tools. Indeed, an accurate reproduction of aerodynamic performance and flow field behaviour during their flight mission represents a crucial aspect for the design of advanced rotary-wing aircraft. In fact, numerical investigation of rotorcraft aerodynamics characterized by complex interactions between the rotors, the wake of the propeller and the wing is typically performed using high-fidelity Navier-Stokes solvers [1]. Nevertheless, the computational effort required by CFD simulations of the entire aircraft precludes their application to a limited number of vehicle configurations. On the other hand, the preliminary design phase of novel rotorcraft requires the investigation of a large number of different configurations reproducing the different phases of their flight mission. In addition, preliminary design of novel aircraft architectures typically includes an aerodynamic optimization study of the lifting surfaces. Therefore, in recent years, the interest of the industrial and scientific community in mid-fidelity aerodynamic solvers has grown in the field of rotorcraft simulations. This interest was finalised to obtain numerical tools that could guarantee a fair good compromise between accuracy and computational costs. Therefore, a thorough assessment of the capabilities of mid-fidelity numerical tools against a such demanding test case as a tiltrotor configuration represents a key aspect for the development of a new approach in the aerodynamic design of innovative rotorcraft vehicles. In particular, considering the design of the control surfaces of a tiltrotor wing, it is important to understand the capabilities of mid-fidelity numerical tools to capture the effects on flow field and on wing/rotor aerodynamic loads due to the presence of the nacelles located at the wingtip nearest to the flaperon region. A proper design of these control surfaces, including the selection of their actuation system, requires a correct evaluation of the aircraft aerodynamic loads during maneuvers, thus enabling to improve the vehicle performance, increasing the efficiency, and reducing the weight and the complexity of the control system. An accurate estimation of the hinge moments of the control surface is one of the fundamental parameters to be assessed, as shown by previous studies by the same authors on the design of control surfaces of a tiltrotor [2, 3].

The present work shows the results of a numerical investigation of a wing with an integrated propeller using the DUST mid-fidelity aerodynamic solver [4]. DUST is an

Presented at the 48th European Rotorcraft Forum, Winterthur, Switzerland, 6-8 September, 2022

open-source software developed by Politecnico di Milano since 2017 for the simulation of interactional aerodynamics of unconventional rotorcraft configurations. The code is released as free software, under the open-source MIT license (`https://www.dust-project.org/`). The code relies on an integral boundary element formulation of the aerodynamic problem and on a vortex particle model [5, 6] of the wakes. A numerical model in DUST can be built using several components, connected to user-defined reference frames, whose position and motion can be defined in a hierarchical way. The presence of different aerodynamic elements allows for different levels of fidelity in the model, ranging from lifting line elements to zero-thickness lifting surfaces and surface panels for thick solid bodies. The simulation evolves in time with a time-stepping algorithm, solving in sequence the Morino-like problem [7] for the potential part of the velocity field, the nonlinear problem for the lifting lines, and updating the rotational part of the velocity field integrating the Lagrangian dynamical equations of the wake particles. A detailed description of the mathematical formulation implemented in DUST is reported in [4].

The wing/propeller model and the test conditions investigated in the present work were released by the Workshop for Integrated Propeller Prediction (WIPP) [8], representing a classical benchmark case for the aerodynamic study of tiltrotors and distributed electrical propulsion aircraft configurations. The main goal of the activity is to assess and to understand the capability of a mid-fidelity aerodynamic solver based on vortex particle method [6], such as DUST, to capture the aerodynamic effects of the installed propeller on the wing, with a particular emphasis on the pressure coefficient and local lift distribution. With this aim, the numerical results obtained by DUST simulations are compared with the experimental data and the results obtained by more accurate numerical aerodynamic models based on the URANS solvers [9]. A further goal of the activity is to evaluate the DUST capabilities to build a robust aerodynamic model of a wing/propeller system, to study the aeroacoustic aspects of this configuration, and to identify the main sources of noise.

2 Wing/propeller model

The WIPP model represents a useful test case for validating aerodynamic codes since an intense experimental campaign was carried out, the results of which constitute a powered wind tunnel test database. The tests took place in the Lockheed Martin Low-Speed Wind Tunnel (LSWT) in Marietta, Georgia, USA as part of the NASA/Armstrong X-57 research program [8]. The model consisted of a 40.5% scale semi-span wing designed for the wind tunnel test campaign to be mounted on the LSWT external balance. The span, from the tunnel floor to the top of the nacelle, is equal to $1.772\,\mathrm{m}$, with a root chord of $0.295\,\mathrm{m}$ and a tip chord of $0.218\,\mathrm{m}$. The wing presents a leading edge sweep of $1.9°$. The model incorporates a nonmetric boundary layer splitter plate $0.163\,\mathrm{m}$ high, which is mounted to the tunnel floor. The model was equipped with an existing C-130 four-blade propeller with a diameter of $0.411\,\mathrm{m}$ and a blade pitch angle of $38°$. The propeller was also used extensively in past activities for testing a 10% scale C-130 aircraft model. The propeller was mounted to a nacelle at the tip of the wing. The nacelle was $0.613\,\mathrm{m}$ long with a maximum diameter of $0.12\,\mathrm{m}$. The accurate geometries, necessary for the construction of the numerical model, were extracted through a digital scan of the wind tunnel model. The latter was equipped with 96 static pressure taps located at six different wing spanwise sections, as shown in Fig. 1. The six sections are reported in Table 1, together with the distance from the propeller axis. Each section included 10 static pressure taps on the upper surface and 6 static pressure taps on the lower surface.

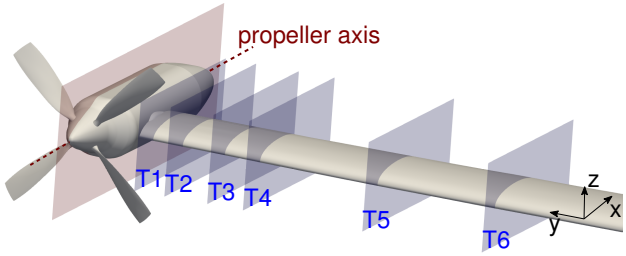

Figure 1: Location of the pressure taps sections on the WIPP model.

Section	Distance
T1	$0.101\,\mathrm{m}$
T2	$0.165\,\mathrm{m}$
T3	$0.256\,\mathrm{m}$
T4	$0.332\,\mathrm{m}$
T5	$0.586\,\mathrm{m}$
T6	$0.840\,\mathrm{m}$

Table 1: Positions of the pressure probe sections.

2.1 DUST numerical model

The DUST numerical model of the WIPP system was built using different aerodynamic elements. Figure 2 illustrates the DUST aerodynamic mesh of the WIPP model, while Tab. 2 summarizes the details of the aerodynamic elements used to mesh the different components of the wing/propeller system.

The wing and the nacelle were modeled as surface panels (SP). Surface panel elements allow to model thick solid bodies, with source and doublet distributions, and following Morino's formulation of the aerodynamic problem a Dirichlet boundary condition for the velocity potential is introduced.

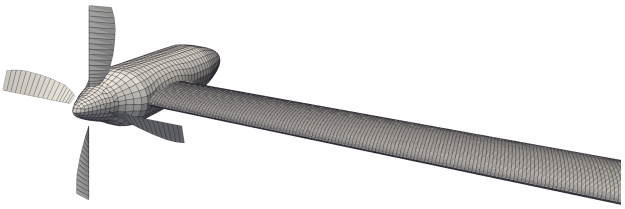

Figure 2: DUST aerodynamic mesh of the WIPP model.

	Elements	
Component	Type	Number
Blade	LL	17×4
Wing	SP	21500
Nacelle	SP	1167
Total		22735

Table 2: Details of aerodynamic elements used to mesh WIPP model with DUST.

The propeller blades were modeled as lifting lines (LL). Lifting lines elements should comprise a single vortex line representing the circulation introduced by a lifting surface, whose intensity is obtained from the tabulated aerodynamic data of the airfoil section they should represent. In DUST they are modeled as a single row of vortex lattice panels with uniform doublet distribution. Thanks to the equivalence between doublet surface distribution and vortex ring, the panels describe both the lifting vortex with the leading edge side, and the beginning of the wake with the remaining sides. While the panels used to model the lifting lines are equal to the ones of the vortex lattice components in terms of singularity distribution and hence in the computation of potential, velocity and gradient induction, there are no conditions imposed on the panels, and their intensity is computed with fixed point iterations to solve the nonlinear problem generated by the introduction of the tabulated aerodynamic data [10]. In the context of this work, the tabulated aerodynamic performances of the propeller airfoils were calculated with 2D simulations performed with the RANS SU2 solver [11], assuming the Spalart-Allmaras turbulence model. Each blade has been modeled with eight airfoils; for each one the aerodynamic coefficients between $-20°$ and $20°$ degrees are computed and subsequently extended between $-180°$ and $180°$ with the method proposed in Ref. [12]. DUST simulations were performed considering a length of 10 propeller revolutions with a time discretisation of $5°$ of the azimuthal angle of the blade. The computational time required to complete the simulation of the WIPP model configuration was about 70 minutes using a workstation with a Dual Intel Xeon Gold 6230R @2.10GHz processor of 104 cores.

3 Results and discussion

In this section, the results of DUST simulations are compared with experimental data from [8] and high-fidelity CFD simulations performed with SU2 software from [9]. In particular, all the CFD simulations data selected for comparison are obtained by the URANS approach over the finest grid considered in the reference work (i.e., G3 grid, see details of the CFD numerical model in [9]). Moreover, the following figure legends retrieve the wind tunnel run indicated in the experimental reference work [8], corresponding to the experimental data set selected for the comparisons.

Run No	Configuration	AoA°	Mach	C_T
187	Isolated Wing	[-10, 20]	0.11	-
30	Wing-Propeller	0	0.04	-
32	Wing-Propeller	0	0.08	-
33	Wing-Propeller	0	0.11	-
80	Wing-Propeller	0	0.11	0.4

Table 3: Details of the experimental runs considered.

Table 3 shows the test conditions corresponding to the experimental runs used for the comparisons. Hereafter, the thrust coefficient is defined as

$$C_T = \frac{T}{\frac{1}{2}\rho V^2 S},$$

where S is the wing reference area equal to $0.4365\,\mathrm{m}^2$.

3.1 Isolated Wing

Firstly, the isolated wing case without the propeller was considered. Figures 3 and 4 show the aerodynamic loads of the wings, ie lift coefficient and polar curves, calculated by DUST and compared with experimental measurements, considering a test condition with Mach equal to 0.11.

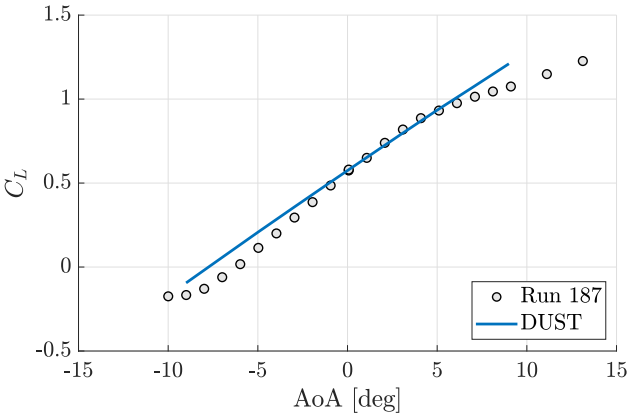

Figure 3: Comparison of the lift coefficient computed for the wing as a function of AoA, Mach=0.11.

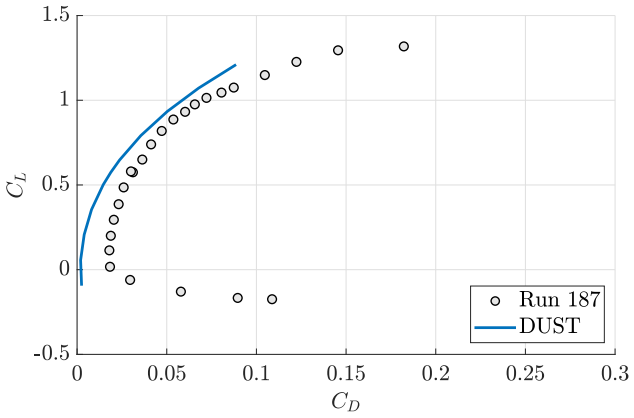

Figure 4: Comparison of the polar curves, Mach=0.11.

For small angles of attack, the lift coefficient obtained with DUST shows a good agreement with the experimental data, while close to the stall the nonlinear effects on the lift curve are not captured, as can be expected considering the assumptions of the numerical method. Since the parasite drag is not modeled by the mid-fidelity solver, there is a discrepancy between the polar curves in the region with a zero lift coefficient. On the other hand, since the induced drag generated by the wing tip vortices is almost well represented, coherence between the curves is recovered as lift increases.

Figures 5,6 and 7 show the pressure coefficient distributions calculated with DUST for the isolated wing on three different wing sections compared with the pressure coefficient measurements (respectively T1, T3, and T6) at two different angles of attack, i.e. AoA=0° and AoA=5°, and Mach number equal to 0.11. The results highlight a very good agreement between the DUST numerical simulations and the experiments, particularly pointing out the suitability of the solver for the wing aerodynamic performance evaluation.

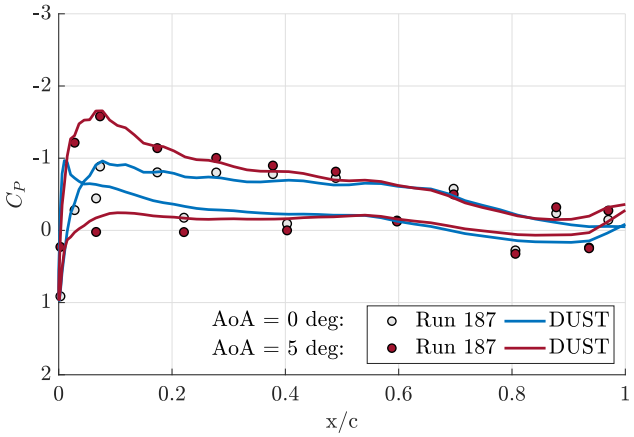

Figure 5: Comparison of the pressure coefficient distribution at section T1 on the isolated wing, Mach=0.11.

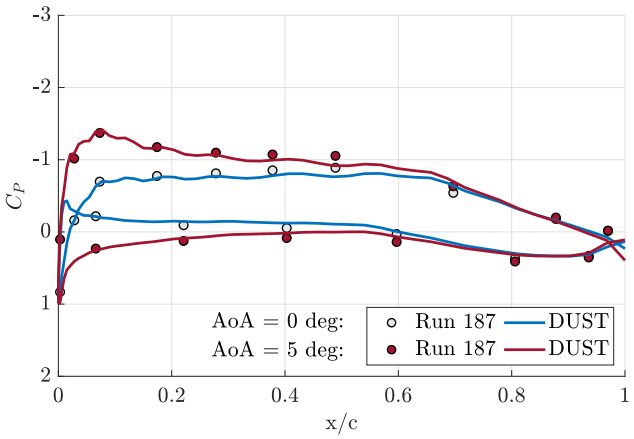

Figure 6: Comparison of the pressure coefficient distribution at section T3 on the isolated wing, Mach=0.11.

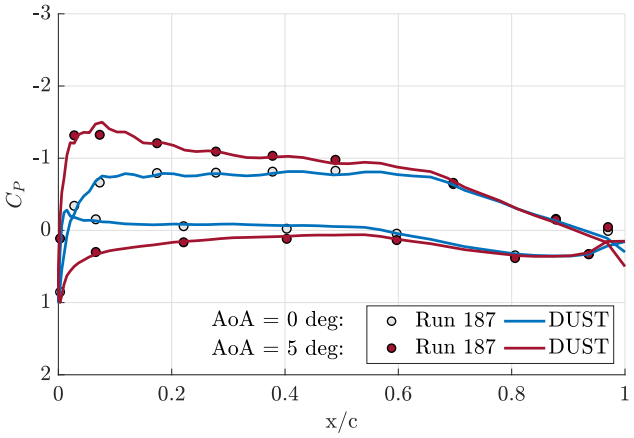

Figure 7: Comparison of the pressure coefficient distribution at section T6 on the isolated wing, Mach=0.11.

3.2 Wing with Integrated Propeller

The complete model with the installed propeller is now considered. In this phase, the DUST capabilities to capture the aerodynamic interactions linked to the propeller wake are tested, both in terms of total loads and pressure coefficient distributions, particularly in the region nearer to the nacelle. In particular, numerical results were also analyzed to identify the effects of the nacelle and propeller on the local sectional airloads of the wing. Finally, DUST capabilities are evaluated to reproduce the complex aerodynamic flow in general and to capture instantaneous pressure fluctuations on the wing.

Figure 8 shows the comparison of the propeller thrust coefficient as a function of the RPM for three different conditions of the Mach number in the free stream. In order to evaluate the capabilities of the mid-fidelity solver to capture the interactional effects on propeller loads due to the wing-nacelle, DUST results are presented here for simulations considering both the isolated propeller as well as for the integrated system.

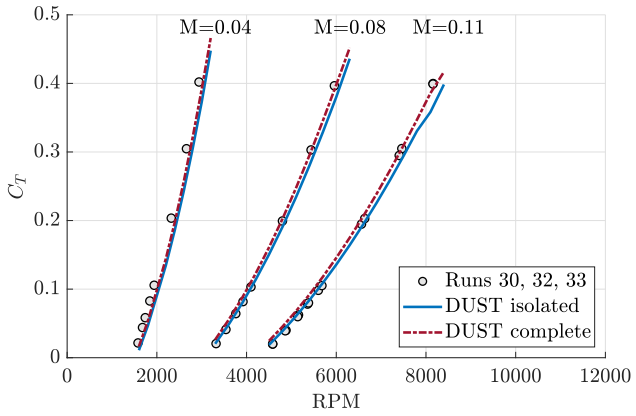

Figure 8: Comparison of the propeller thrust coefficient as a function of angular velocity for different free-stream Mach number.

Very good agreement with the experimental data was found for all three free-stream Mach numbers considered. In particular, DUST results show that the wing-nacelle system interaction provides a slight additional thrust on the propeller, that is appreciable with the DUST approach and gets numerical results nearer to the experimental ones, particularly at higher RPM.

Figures 9,10 and 11 show the comparison of the pressure coefficient distributions on the wing for the complete model equipped with nacelle and propeller at three different sections for AoA=$0°$. Considering the pressure comparison in section T1, i.e. the closest to the propeller, thus highlighting the highest interactional effects on the wing, the CFD data are in quite good agreement with experiments, while the DUST results present some discrepancies. In particular, the suction peak level on the upper surface of the wing is slightly underestimated by DUST, as well as a lower and quite flatter pressure distribution is observed over the lower surface of the wing at this section with respect to the CFD and experimental data. On the other hand, DUST results quite well resume the pressure behavior obtained by both CFD and experiments on sections T3 and T6.

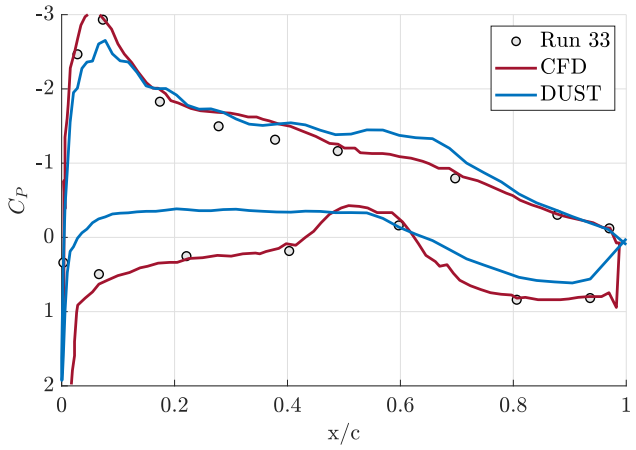

Figure 9: Comparison of the pressure coefficient distribution at section T1 on the wing for the complete WIPP model, AoA=$0°$, Mach=0.11.

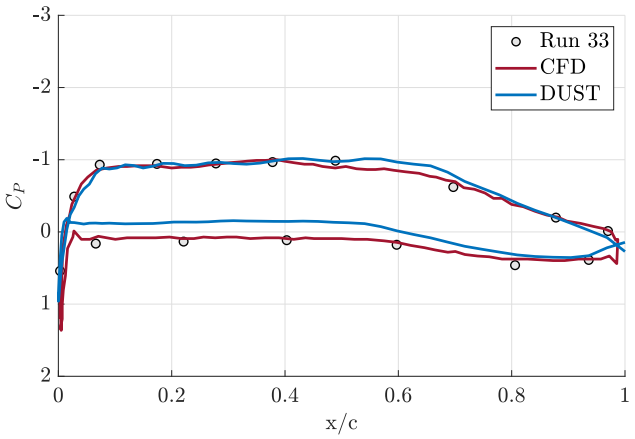

Figure 10: Comparison of the pressure coefficient distribution at section T3 on the wing for the complete WIPP model, AoA=$0°$, Mach=0.11.

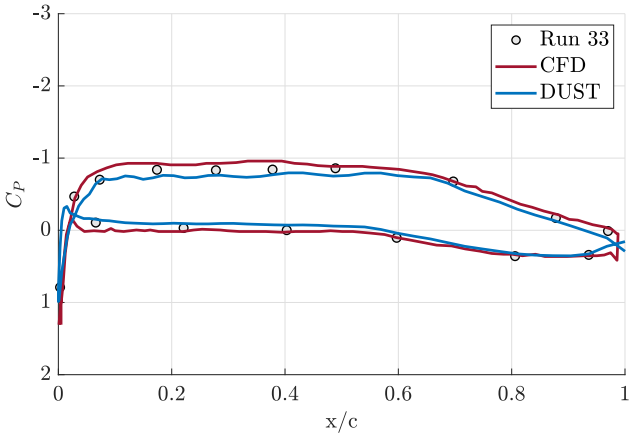

Figure 11: Comparison of the pressure coefficient distribution at section T6 on the wing for the complete WIPP model, AoA=$0°$, Mach=0.11.

Indeed, on section T3 only a slight underestimation of the pressure coefficient is observed on the wing lower surface, while the agreement on wing upper surface distribution is satisfactory. Similar results are observed at section T6 as well.

The validation against experimental data opened the opportunity to use numerical results obtained with DUST to analyse the effects of the nacelle and propeller on the local aerodynamic performance of the wing. With this aim, Figs. 12,13 and 14 show the comparison of the pressure coefficient distributions computed by DUST on three wing sections adding the nacelle and the propeller to the numerical model of the wing. In particular, on section T1 and T2 the effect of the propeller is remarkable. Indeed, the high-velocity air blown by the propeller provides an apparent increase of suction on the wing upper surface, particularly for the sections nearer to the propeller. Furthermore, an increase in pressure coefficient is observed on the lower surface of the wing, close to the trailing edge region, due to the propeller effect. Consequently, the propeller provides a local increase

of the lift coefficient in the outer region of the wing.

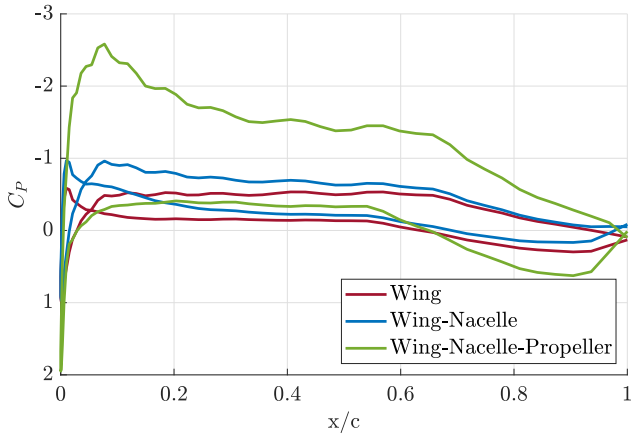

Figure 12: Comparison of the numerical pressure coefficient distribution at section T1 on the wing for different model configurations, AoA=0°, Mach=0.11.

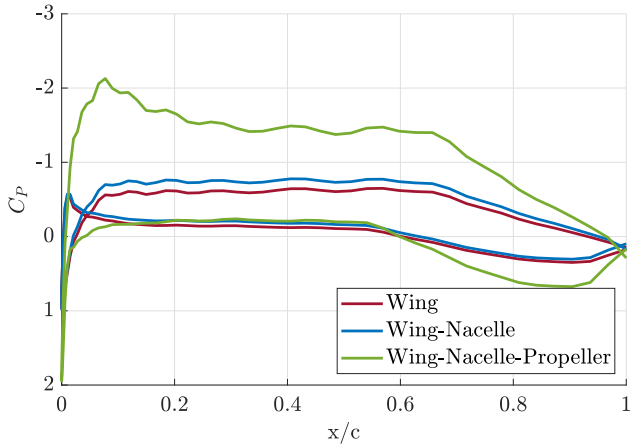

Figure 13: Comparison of the numerical pressure coefficient distribution at section T2 on the wing for different model configurations, AoA=0°, Mach=0.11.

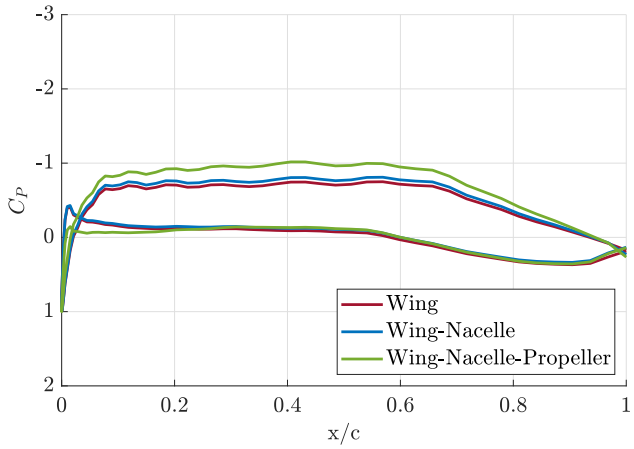

Figure 14: Comparison of the numerical pressure coefficient distribution at section T3 on the wing for different model configurations, AoA=0°, Mach=0.11.

A similar effect on the upper surface of the wing for sections T1 and T2 can be observed due to the nacelle only. Indeed, the local curvature of the nacelle provides an acceleration of the flow in the outer wing region, thus slightly increasing the suction on the upper surface of the wing. The comparison of pressure coefficient distribution on section T3, further from the propeller, confirms the trend observed for the wing outer sections, but here the effects of the nacelle and of the propeller are, as expected, quite lower.

The analysis of the results follows by evaluating the capabilities of DUST to represent the flow field. With this aim, Figs. 15 to 19 show the comparison of the profiles of the free-stream velocity component U evaluated at five wake stations downstream the propeller. In particular, the experimental wake data are measured at $0.0673\,\mathrm{m}$, $0.1562\,\mathrm{m}$, $0.3594\,\mathrm{m}$, $0.5626\,\mathrm{m}$, and $1.076\,\mathrm{m}$ downstream from the propeller disk [8]. CFD data obtained by URANS simulations were not available for the fifth station [9]. The quantitative comparison of the velocity profiles highlights two main features. The first is that the behavior of the wake profiles computed with DUST quite well resumes the representation obtained by high-fidelity CFD.

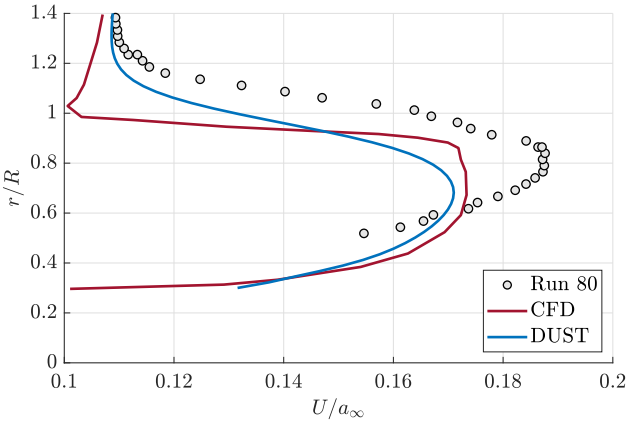

Figure 15: Comparison of the free-stream velocity component profiles at x = $0.0673\,\mathrm{m}$, complete WIPP model, Mach=0.11.

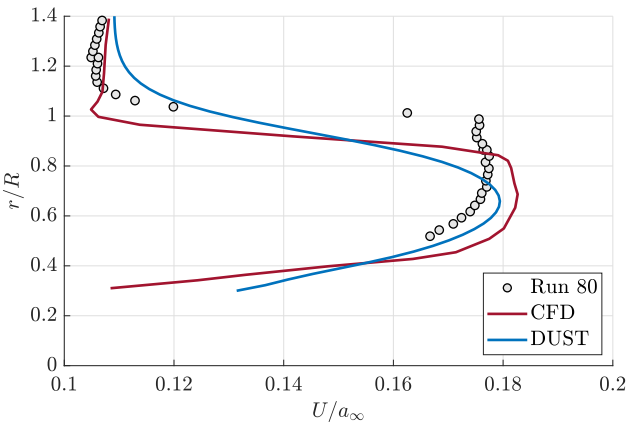

Figure 16: Comparison of the free-stream velocity component profiles at x = $0.1562\,\mathrm{m}$, complete WIPP model, Mach=0.11.

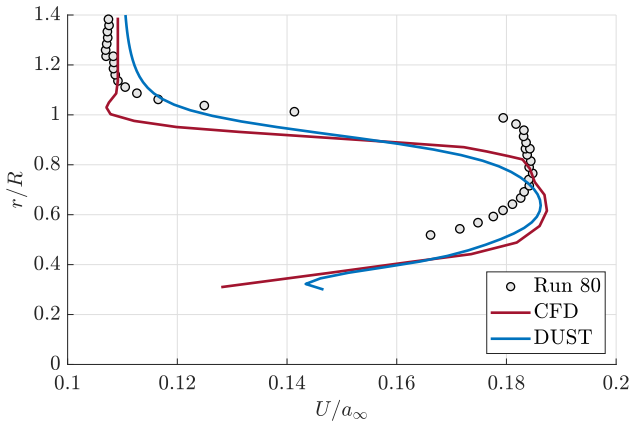

Figure 17: Comparison of the free-stream velocity component profiles at x = $0.3594\,\mathrm{m}$, complete WIPP model, Mach=0.11.

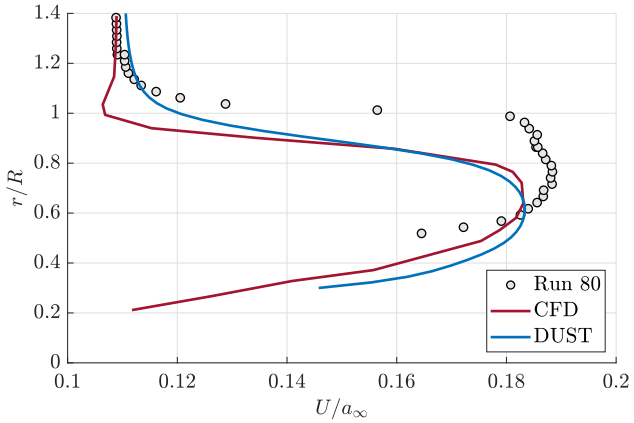

Figure 18: Comparison of the free-stream velocity component profiles at x = $0.5626\,\mathrm{m}$, complete WIPP model, Mach=0.11.

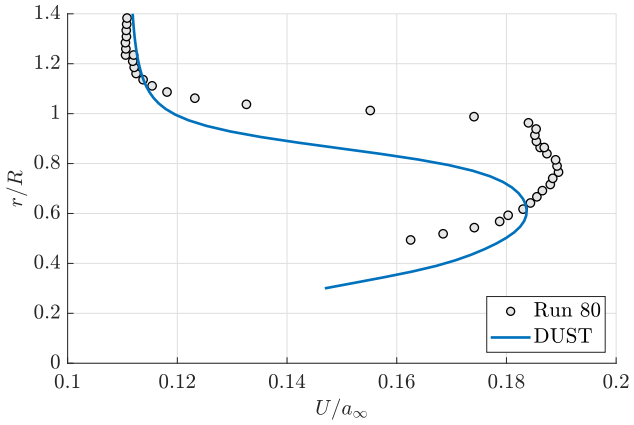

Figure 19: Comparison of the free-stream velocity component profiles at x = $1.076\,\mathrm{m}$, complete WIPP model, Mach=0.11.

The second is that both the mid-fidelity and the high-fidelity numerical approaches evaluate a downward deflection of the velocity deficit in the propeller wake with respect to experimental data. This aspect is, indeed, commonly observed on almost all the wake stations considered for the comparison.

A global visualization of the flow field computed by DUST around the complete WIPP model is provided in Fig. 20, showing the Q-criterion isosurface colored by the nondimensional free-stream velocity component and the contours of pressure coefficient on the model surface. The flow representation clearly shows the DUST capability to capture the interaction of the helical structure generated by the propeller blade tip vortices with the wing-nacelle surface. Moreover, DUST numerical solution appreciates also a secondary helical vortical structure generated from blades trailing edge interacting with the nacelle surface. The footprint of these vortical structures on wing-nacelle surface can be observed in Fig. 21 showing the contours of the instantaneous pressure fluctuations computed by DUST. In particular, an alternate dotted pressure pattern due to the impinging of the blade tip vortices structure is clearly visible from DUST results on the outboard portion of the wing. Moreover, a streaked pressure pattern can be observed on the nacelle surface as a result of the secondary vortex structure interaction.

These results highlight very similar features with respect to high-fidelity CFD approach [9] and suggest that the DUST numerical model would allow a good identification of the possible noise sources related to the wing-propeller interaction, thus encouraging the use of this mid-fidelity approach to investigate the aeroacoustics of similar configurations. In particular, thanks to the very low computational effort required by DUST simulations, the mid-fidelity approach could be successfully used for the aerodynamic and aeroacoustic optimization of novel wing-propeller configurations.

4 Conclusions

The present paper described a numerical activity aimed to investigate the capabilities of a vortex particle-based aerodynamic solver as DUST to investigate the wing-propeller aerodynamic interaction, representing a typical feature of novel AAM aircraft concepts. With this aim, a wing-propeller model widely investigated in the literature was selected, and the results of the DUST numerical simulations were compared with both experimental data and recent high-fidelity CFD simulations. The results of the analysis highlighted a fairly good agreement of the DUST calculations for both the evaluation of the propeller load and the distribution of pressure on the wing. A certain discrepancy with respect to CFD data was observed locally only in the wing region nearest to propeller, where interactional effects are higher. Furthermore, the comparison of the pressure distributions calculated by adding the different elements of the model showed the ability to evaluate the effects of the nacelle and the propeller on the aerodynamic performance of the wings. The flow field analysis made by the quantitative comparison of free-stream velocity profiles and by the overall representation of the flow around the wing-propeller system highlighted DUST capabilities to capture the main interactional features

of this configuration responsible for noise generation, similarly to what was found with a high-fidelity CFD approach but with a quite lower computational effort. Consequently, the present work encourages the use of the mid-fidelity numerical approach implemented in DUST for aerodynamics and aeroacoustic studies as well as for the optimization of wing-propeller configurations typical of novel AAM aircraft concepts.

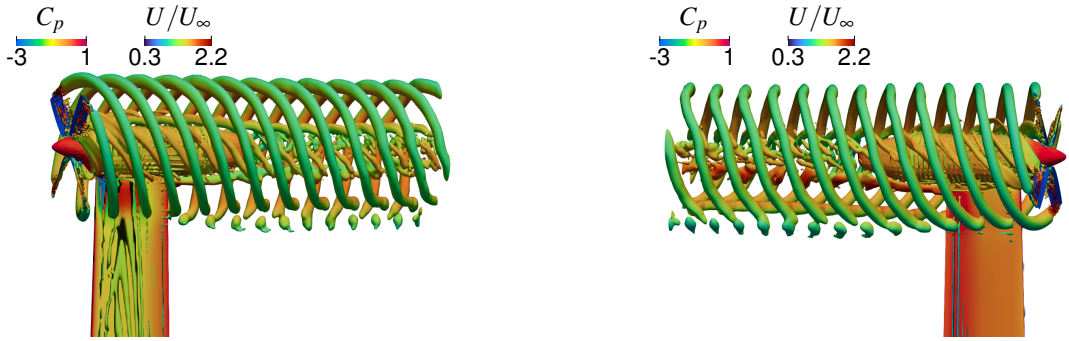

Figure 20: Visualization of the flow field computed by DUST around the complete WIPP model: Q-criterion iso-surface colored by the non-dimensional free-stream velocity component and contours of pressure coefficient on the model surface (top and bottom views), M_∞=0.11, C_T=0.4, AoA=0°

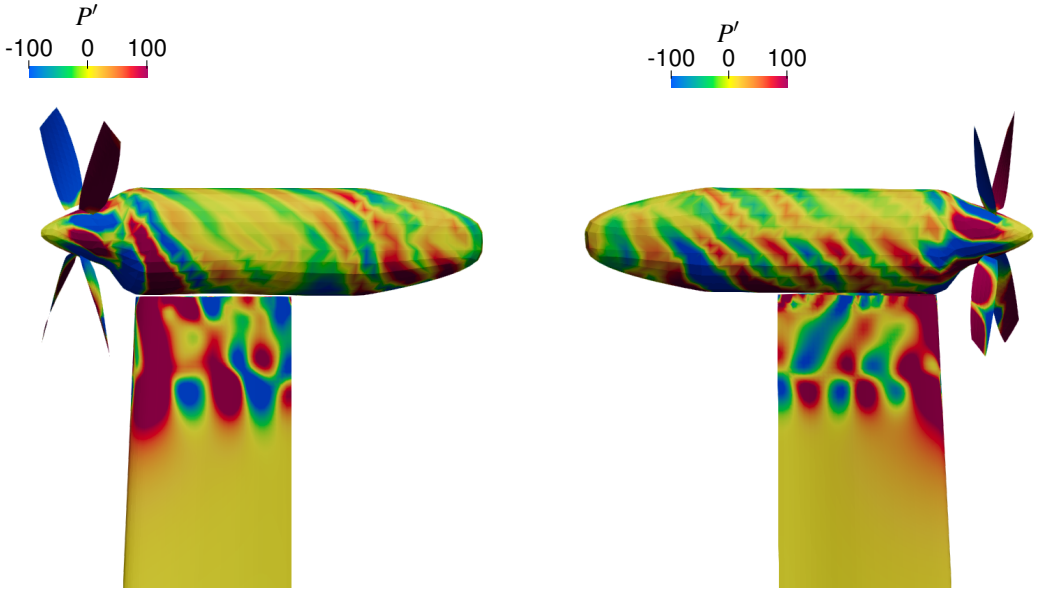

Figure 21: Instantaneous pressure fluctuations computed by DUST (top and bottom views), M_∞=0.11, C_T=0.4, AoA=0°.

Acknowledgments

This project has received funding from the Clean Sky 2 Joint Undertaking (JU) under grant agreement No 863418. The JU receives support from the European Union's Horizon 2020 research and innovation programme and the Clean Sky 2 JU members other than the Union.

The research leading to these results has received funding from the Clean Sky 2 – H2020 Framework Programme, under the grant agreement N.885971, (the FORMOSA project).

Copyright Statement

References

[1] Joon Lim and Steven Tran. Interactional structural loads of the xv-15 rotor in airplane mode. In *45th European Rotorcraft Forum (ERF 2019)*, pages 1–10, 2019.

[2] Alberto Savino, Alessandro Cocco, Alex Zanotti, Matteo Tugnoli, Pierangelo Masarati, and Vincenzo Muscarello. Coupling mid-fidelity aerodynamics and multibody dynamics for the aeroelastic analysis of rotary-wing vehicles. *Energies*, 14(21):6979, 2021.

[3] A. Savino, A Cocco, A. Zanoni, A. De Gaspari, Alex Zanotti, J. Cardoso, D. Carvalhais, and V. Muscarello. Design and optimization of innovative tiltrotor wing control surfaces through coupled multibody-mid-fidelity aerodynamics simulations. In *Vertical Flight Society's 78th Annual Forum & Technology Display*, 2022.

[4] Matteo Tugnoli, Davide Montagnani, Monica Syal, Giovanni Droandi, and Alex Zanotti. Mid-fidelity approach to aerodynamic simulations of unconventional vtol aircraft configurations. *Aerospace Science and Technology*, 115:106804, 2021.

[5] G. S. Winckelmans. *Topics in vortex methods for the computation of three-and two-dimensional incompressible unsteady flows*. Ph.D. dissertation, California Institute of Technology, 1989.

[6] G. H. Cottet and P. D. Koumoutsakos. *Vortex methods: theory and practice*. Cambridge University Press, 2000.

[7] L. Morino and C.-C. Kuot. Subsonic potential aerodynamics for complex configurations: A general theory. *AIAA Journal*, 12(2):191–197, 1974. doi:10.2514/3.49191.

[8] John R Hooker, Andrew Wick, Starr R Ginn, Jimmy Walker, and Benjamin T Schiltgen. Overview of low speed wind tunnel testing conducted on a wingtip mounted propeller for the workshop for integrated propeller prediction. In *AIAA AVIATION 2020 FORUM*, page 2673, 2020.

[9] Beckett Yx Zhou, Myles Morelli, Nicolas R Gauger, and Alberto Guardone. Simulation and sensitivity analysis of a wing-tip mounted propeller configuration from the workshop for integrated propeller prediction (wipp). In *AIAA AVIATION 2020 FORUM*, page 2683, 2020.

[10] S Gallay and E Laurendeau. Nonlinear generalized lifting-line coupling algorithms for pre/poststall flows. *AIAA Journal*, 53(7):1784–1792, 2015.

[11] Thomas D Economon, Francisco Palacios, Sean R Copeland, Trent W Lukaczyk, and Juan J Alonso. Su2: An open-source suite for multiphysics simulation and design. *Aiaa Journal*, 54(3):828–846, 2016.

[12] Lorenzo Battisti, Luca Zanne, Marco Raciti Castelli, Alessandro Bianchini, and Alessandra Brighenti. A generalized method to extend airfoil polars over the full range of angles of attack. *Renewable Energy*, 155:862–875, 2020.